

# Spatiotemporal control of cell signalling using a light-switchable protein interaction

Anselm Levskaya<sup>1,2,3</sup>, Orion D. Weiner<sup>1,4</sup>, Wendell A. Lim<sup>1,5</sup> & Christopher A. Voigt<sup>1,3</sup>

Genetically encodable optical reporters, such as green fluorescent protein, have revolutionized the observation and measurement of cellular states. However, the inverse challenge of using light to control precisely cellular behaviour has only recently begun to be addressed; semi-synthetic chromophore-tethered receptors<sup>1</sup> and naturally occurring channel rhodopsins have been used to perturb directly neuronal networks<sup>2,3</sup>. The difficulty of engineering light-sensitive proteins remains a significant impediment to the optical control of most cell-biological processes. Here we demonstrate the use of a new genetically encoded light-control system based on an optimized, reversible protein–protein interaction from the phytochrome signalling network of *Arabidopsis thaliana*. Because protein–protein interactions are one of the most general currencies of cellular information, this system can, in principle, be generically used to control diverse functions. Here we show that this system can be used to translocate target proteins precisely and reversibly to the membrane with micrometre spatial resolution and at the second timescale. We show that light-gated translocation of the upstream activators of Rho-family GTPases, which control the actin cytoskeleton, can be used to precisely reshape and direct the cell morphology of mammalian cells. The light-gated protein–protein interaction that has been optimized here should be useful for the design of diverse light-programmable reagents, potentially enabling a new generation of perturbative, quantitative experiments in cell biology.

A quantitative understanding of living cells will require methods to perturb and control the activities of their constituent proteins at fine spatial and temporal resolutions. By measuring responses to precise perturbations, predictive models of cellular networks can be tested and iteratively improved<sup>4,5</sup>. A promising approach is to couple the activity of targeted proteins to light signals, either by incorporating photoactive allosteric modulators semisynthetically<sup>1,6,7</sup>, or by exploiting naturally occurring light-sensitive domains<sup>2,3,8–10</sup>. A particularly useful light-sensitive interaction for creating a general genetically encoded light-control system for cell biology comes from the phytochrome signalling network of plants.

Phytochromes are photoreceptive signalling proteins responsible for mediating many light-sensitive processes in plants, including seed germination, seedling de-etiolation and shade avoidance<sup>11</sup>. They detect red and near-infrared light through the photoisomerization of a covalently bound tetrapyrrole chromophore such as phycocyanobilin (PCB)<sup>11</sup>. This photoisomerization event is coupled to an allosteric transition in the phytochrome between two conformational states called Pr (red-absorbing) and Pfr (far-red-absorbing) (Fig. 1a). In one well studied signalling pathway, upon stimulation with red (650 nm) light, the *Arabidopsis thaliana* phytochrome B (PhyB) protein binds directly to a downstream transcription factor, phytochrome interaction factor 3 (PIF3), translocates to the nucleus as a

heterodimer and directly modulates the transcription of response genes. PIF3 binds only the red-light-exposed form of phytochrome, Pfr, and shows no measurable binding affinity for the dark- or infrared-exposed Pr state<sup>12</sup>. Thus, this interaction can be reversed by infrared

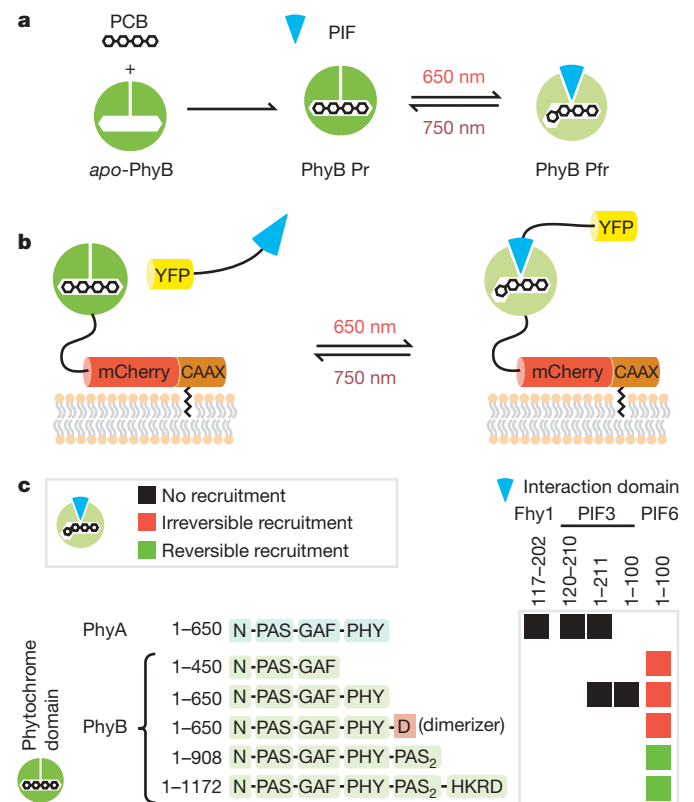


**Figure 1 | The phytochrome–PIF interaction can be used to reversibly translocate proteins to the plasma membrane in a light-controlled fashion.** **a**, apo-PhyB covalently binds to the chromophore phycocyanobilin (PCB) to form a light-sensitive holoprotein. PhyB undergoes conformational changes between the Pr and Pfr states catalysed by red and infrared light, reversibly associating with the PIF domain only in the Pfr state. **b**, This heterodimerization interaction can be used to translocate a YFP-tagged PIF domain to PhyB tagged by mCherry and localized to the plasma membrane by the C-terminal CAAX motif of Kras. **c**, Phytochrome and PIF domains functional in mammalian cells were tested for reversible light-dependent recruitment of YFP to the plasma membrane using confocal microscopy. Previously published PIF constructs either failed to show visible recruitment or showed irreversible recruitment. Only PhyB constructs harbouring tandem PAS repeats (unique to the plant phytochromes) showed detectable but reversible recruitment *in vivo*.

<sup>1</sup>The Cell Propulsion Lab, UCSF/UCB NIH Nanomedicine Development Center, <sup>2</sup>Graduate Program in Biophysics, <sup>3</sup>Department of Pharmaceutical Chemistry, <sup>4</sup>Cardiovascular Research Institute, <sup>5</sup>Howard Hughes Medical Institute and Department of Cellular and Molecular Pharmacology, University of California, San Francisco, California 94158-2517, USA.

light. This light-sensitive interaction has been mapped to the 650-residue amino-terminal photosensory core of PhyB and a conserved 100-residue N-terminal activated phytochrome binding (APB) domain of PIF3 (ref. 13).

In previous work, this light-sensitive interaction has been used in yeast to construct a photoreversible two-hybrid transcriptional activator to tune the expression level of a targeted reporter gene<sup>10</sup>, to target split intein domains to titrate the conditional protein splicing of a reporter gene<sup>14</sup>, and *in vitro* to target directly Cdc42 to its effector WASP to regulate actin nucleation<sup>15</sup>. Collectively this work suggests that the PhyB–PIF interaction can be functionally coupled to a wide variety of signalling processes through engineered fusion proteins.

So far, however, no reported system using the PhyB–PIF interaction has been demonstrated to enable fine spatiotemporal control of dimerization *in vivo*. Indeed, the relatively weak binding strength and slow reverse kinetics of the reported domains<sup>15</sup> have prevented us from successfully applying these earlier interaction pairs for *in vivo* control of signalling. We have optimized the phytochrome interaction to enable its spatiotemporal control in experiments with live mammalian cells.

We first confirmed that PhyB could covalently bind externally supplied PCB chromophore in mammalian cells by using a PhyB mutant (Y276H) that fluoresces at far-red frequencies in the PCB-coupled state only<sup>16</sup>. NIH3T3 cells transfected with this construct show fluorescence after only 30 min of exposure to 5  $\mu\text{M}$  PCB, confirming rapid autoligation at physiological conditions (Supplementary Fig. 1). Multiple potential phytochrome–PIF pairs were screened by a fluorescence translocation assay in NIH3T3 cells with confocal microscopy. We measured the red-light-induced translocation of yellow fluorescent protein (YFP) fused to PIF domains to co-expressed phytochrome domains fused through a flexible linker to mCherry and localized to the plasma membrane by a carboxy-terminal polybasic, prenylation sequence from Kras<sup>17</sup> (Fig. 1b). Of all previously reported PIF domains<sup>13,18,19</sup>, only the N terminus of PIF6 is strong enough to cause significant translocation of YFP to the membrane (Fig. 1c). However, its interaction with the PhyB photosensory core (residues 1–650) is irreversible in infrared light. Assaying it against different variants of PhyB revealed that the tandem C-terminal PAS domains of plant phytochromes are necessary to confer rapid photoreversibility under infrared light, underlining the importance of a previously reported autoinhibitory interaction for phytochrome signalling<sup>20</sup>. We refer to the optimized, reversible PhyB–PIF6 interaction simply as the ‘Phy–PIF’ interaction.

Using this optimized Phy–PIF pair we observe rapid translocation to the plasma membrane under dilute red light (650 nm,  $20 \mu\text{mol m}^{-2} \text{s}^{-1}$ ) and from the membrane under infrared light ( $>750 \text{ nm}$ ,  $300 \mu\text{mol m}^{-2} \text{s}^{-1}$ ) (Fig. 2a and Supplementary Movies 1 and 2). Kinetic measurements of the Phy-induced cytoplasmic depletion of PIF–YFP under maximum illumination yield translocation time constants of  $1.3 \pm 0.1 \text{ s}$  (s.d.  $n = 3$ ) for membrane recruitment and  $4 \pm 1 \text{ s}$  (s.d.  $n = 3$ ) for membrane release (Fig. 2a and Supplementary Fig. 2), demonstrating second-timescale control. These rates are an order of magnitude faster than previous chemically induced translocation systems<sup>21</sup> and are very near the physical limits for whole-cell diffusion (see calculation in Supplementary Information). The Phy–PIF translocation proved very robust—it could be cycled over a hundred times by alternating red and infrared illumination with no measurable decrease in recruitment ratios over time, despite many cycles of imaging at photon fluxes far higher than those phytochromes are exposed to in natural lighting conditions (Fig. 2b and Supplementary Movie 3).

The rapid forward and reverse kinetics of our Phy–PIF pair allow for fine spatial control of membrane recruitment by simultaneously exposing cells to patterned light at the two antagonizing wavelengths. In NIH3T3 cells co-expressing the above Phy–Kras(CAAX) and PIF–YFP recruitment pair, a nitrogen dye cell laser was used to deliver pulses of ‘activating’ red light (650 nm, 20 Hz) to a focused point on the sample plane, while the whole sample was bathed in continuous

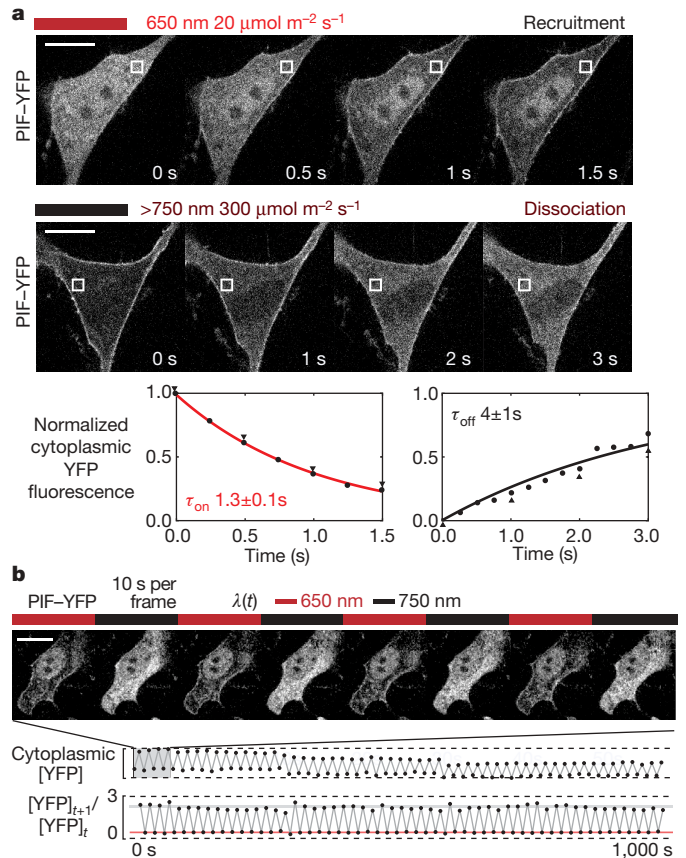


**Figure 2 | Confocal microscopy demonstrating the second-scale kinetics and photostability of the Phy–PIF photoswitchable membrane recruitment system.** **a**, Confocal microscopy of NIH3T3 cells reveals rapid translocation of YFP between cytosol and plasma membrane under red and infrared light. Fitting exponentials to the cytoplasmic depletion of YFP gives typical time constants of  $1.3 \pm 0.1 \text{ s}$  for recruitment and  $4 \pm 1 \text{ s}$  for dissociation ( $n = 3$ ). White rectangles show regions sampled for plotted traces. Arrowheads in graphs mark the time points shown (Supplementary Movies 1 and 2). **b**, Rapid alternation between the 650 and 750 nm light can generate oscillations in the cytoplasmic concentrations of YFP. Absolute cytoplasmic concentration of YFP for this series is plotted along with the ratio change between time points to adjust for photobleaching and cell drift. The red and grey bars represent the standard deviations of the recruited and released cytosolic fluorescence, demonstrating near-fixed recruitment ratios over more than a hundred iterations (Supplementary Movie 3). Scale bars in **a** and **b**,  $20 \mu\text{m}$ .

‘inactivating’ infrared light obtained by filtering the microscope bright-field source ( $>750 \text{ nm}$ ) (Fig. 3a). When the cell membrane is imaged by total internal reflectance (TIRF) microscopy we observe a sharp spot of membrane-localized YFP several micrometres in diameter around the irradiated point (Fig. 3c). The rapid ‘off’ kinetics of the Phy–PIF interaction traps the membrane-recruited YFP pool to this spot, as any YFP diffusing away is dissociated from the membrane by the surrounding infrared light. This spot of recruited YFP can be rapidly relocated across the cell by repositioning the point of incident light (Supplementary Movie 4).

We developed a second, fully automated method of controlling the distribution of both light frequencies on the cell membrane by using a digital micromirror array to project patterned light on to the sample plane of the microscope at micrometre resolutions<sup>22</sup>. By irradiating the sample with 650-nm and 750-nm light sources oriented to take advantage of both micromirror angle states, a complementary two-colour red/infrared pattern can be projected on to the sample plane, allowing one to ‘paint’ high-resolution inverse distributions of Pfr and Pr phytochrome on to the membrane of the cell (Fig. 3b). We were able to project faithfully a simple pixel-based movie into the

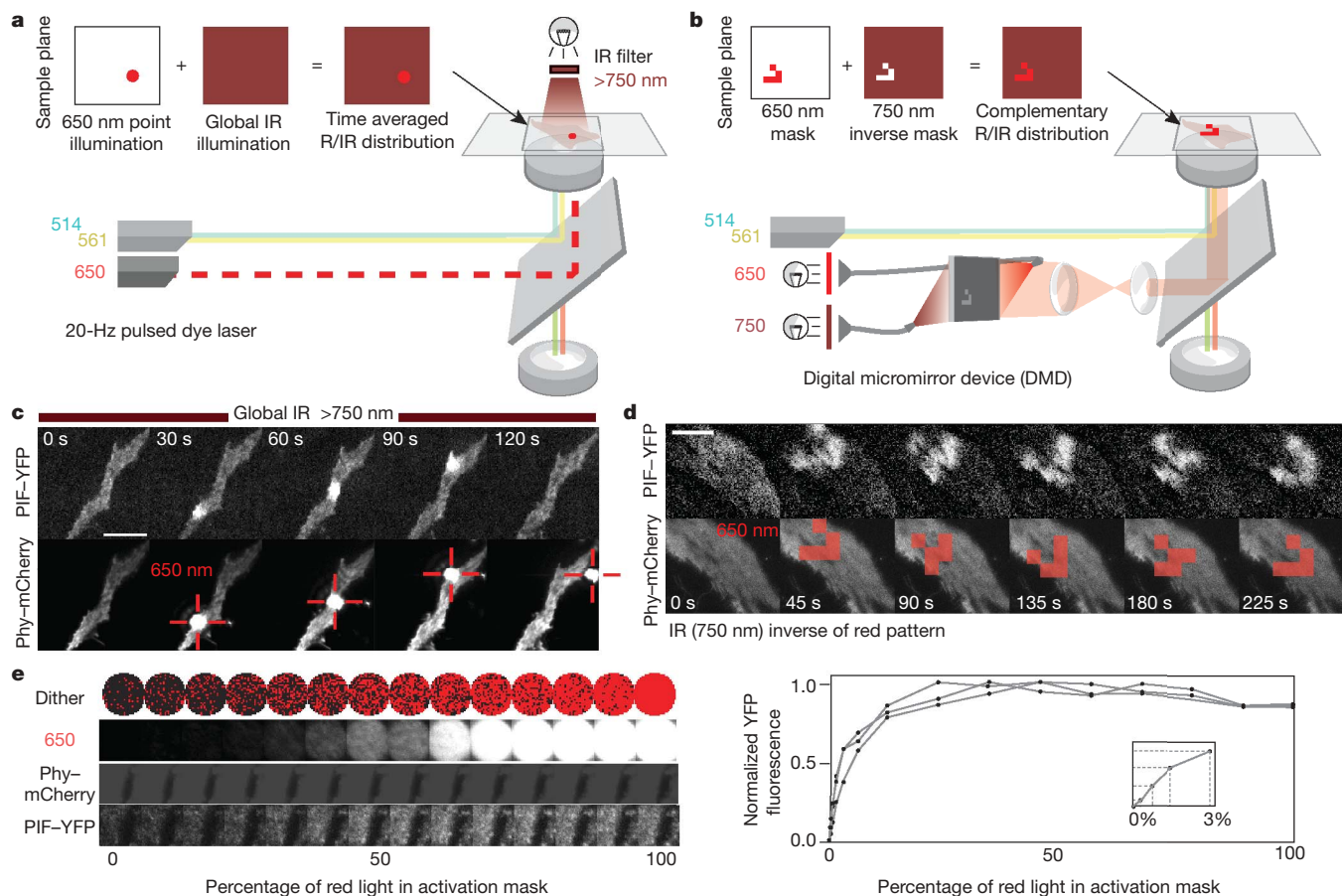


**Figure 3 | Recruitment to the plasma membrane can be controlled spatially by simultaneously irradiating cells with patterned red and infrared light.**

**a**, A nitrogen dye cell laser exciting a 650-nm rhodamine dye was focused on to the sample plane of the microscope at 20 Hz while infrared (IR)-filtered white light continuously bathed the entire sample. **b**, A digital micromirror device focused on to the sample plane was used to send high-resolution patterns of 650 nm/750 nm light from a DG-4 source into the microscope under software control. This results in complementary red and infrared distributions on the sample plane. **c**, TIRF imaging of localized membrane recruitment by a point source as in **a** shows highly localized YFP recruitment (Supplementary Movie 4). The recruited YFP spot's diameter is roughly

membrane-recruited PIF-YFP distribution of a NIH3T3 cell. TIRF imaging reveals fine features at five micrometres, demonstrating an unprecedented degree of control over protein localization in living cells (Fig. 3d and Supplementary Movie 5). Additionally, by dithering the average amount of red light in the target mask through software, we could smoothly titrate the fraction of active Phy and recruited PIF-YFP, demonstrating effective 'greyscale' control of the chemical potential (Fig. 3e and Supplementary Movie 6). Using this data, we estimate the *in vivo* dissociation constant of the PhyB-PIF6 interaction to be approximately  $K_d = 20\text{--}100$  nM (Supplementary Fig. 5).

We were motivated to engineer a membrane recruitment system because many signalling proteins are, at least in part, activated by interactions that relocate them to the membrane. Moreover, plasma membrane recruitment systems have been successfully used as a platform for small-molecule-induced chemical biology control systems<sup>21,23–25</sup>. For example, chemically induced membrane translocation of the Rho- and Ras-family small G proteins<sup>21,23</sup> or the guanine nucleotide exchange factors (GEFs) that activate them<sup>21</sup> can generate global morphological changes. We reasoned that Phy-PIF-induced translocation might generate similar morphological changes, but with much higher spatial and temporal resolution. We chose to focus on spatiotemporal control of the Rho-family GTPases Rac1, Cdc42 and RhoA, given their central role in the

dynamic spatial regulation of the actin cytoskeleton at the polarized edges of motile cells (Fig. 4a). Gated-recruitment constructs were made from the isolated catalytic modules (the DH-PH domain) of the RacGEF Tiam, the Cdc42GEF intersectin and the RhoGEF Tim. The optimal construct topologies for DH-PH activation were found by screening for Tiam-DH-PH activity via the global morphological changes that occurred in transfected, serum-depleted NIH3T3 cells when the entire field was exposed to red light. Global recruitment of the optimal PIF-Tiam-DH-PH chimera caused a pronounced lamellipodial phenotype within 20 min in most (>80%) co-transfected cells, compared to PIF-YFP-only recruitment or control cells lacking the PCB chromophore (Fig. 4b). This potent effect of recruiting the Tiam GEF activity to the membrane is similar to that observed using chemical dimerizers<sup>21</sup>. We further tested the generality of this construct topology by confirming that global RhoGEF recruitment induced cell body contraction in fibroblasts (Supplementary Movie 9).

Given the strong global morphological effects of Tiam DH-PH domain membrane translocation, we then tested the effects of spatially localized light-activated translocation. Red laser stimulation was used for localized recruitment of the Tiam DH-PH domain in serum-depleted NIH3T3 cells (within a background of global repression by infrared light), effecting within 5–10 min a localized lamellipodial

3  $\mu\text{m}$  and can be quickly moved by repositioning the laser. The final frame shows that the YFP spot is not merely bleed-through of the excitatory laser light, but genuine local fluorescent protein recruitment. **d**, TIRF movies of structured membrane recruitment by programmatically updating masks for red and infrared light using a digital micromirror device as in **b** were collected, revealing a faithful reproduction in the recruited YFP distribution of a movie of the cellular automaton 'game-of-life glider' that was projected (Supplementary Movie 5). **e**, Images show the raw traces of titrated input 650-nm light and recruited PIF-YFP. The plot (right panel) shows the recruitment level as a function of 650-nm ratio for three typical experiments. Inset shows the non-saturated regime. Scale bars, 20  $\mu\text{m}$ .

Normalized YFP fluorescence

Percentage of red light in activation mask



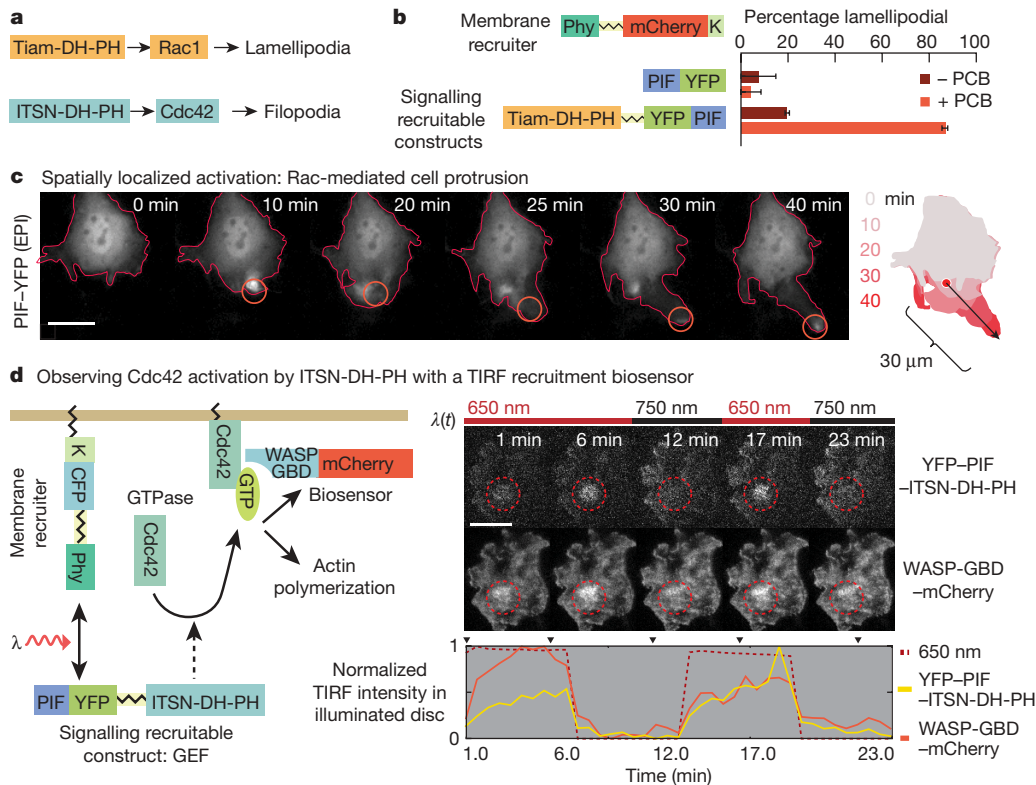


**Figure 4 | Rho-family G-protein signalling can be controlled by the light-activated translocation system.** **a**, The catalytic DH-PH domains of RhoGEFs Tiam and intersectin (ITSN) activate their respective G proteins Rac1 and Cdc42, which in turn act through effector proteins to modify the actin cytoskeleton. **b**, Recruitable constructs with Tiam DH-PH domains were assayed for their ability to induce lamellipodia in NIH3T3 cells by exposing serum-depleted cells transfected with the indicated constructs to red (650 nm) light and counting the percentage of cells that produced lamellipodia within 20 min under live microscopy. Error bars indicate s.e.m. ( $n = 2$ , average 30 cells;  $P$ -value = 0.0004 for Tiam). **c**, Local induction and

'bloom' (Supplementary Movie 8). By slowly extending the point of activating light away from the cell, it is even possible to 'draw out' an extended process up to 30 μm from the main body of the cell that is stable after the light has been withdrawn. This indicates the future possibility of programmatically specifying cell geometries and inter-cellular connections with light (Fig. 4c and Supplementary Movies 7 and 8).

We further verified the signalling activity of our PIF-DH-PH reagents by verifying that point induction causes local, transient increases of the active form of GTPase as measured by the membrane enrichment of biosensors—either mCherry-tagged GBD-binding domains from WASP (Fig. 4d and Supplementary Movie 11) or PAK (Supplementary Fig. 4)—by TIRF microscopy. Using these biosensors we see that GTPase activation occurs rapidly, within seconds, indicating that a subsequent signalling step is responsible for the typical delay of 5–10 min for lamellipodial and filopodial protrusions.

We have developed a genetically encoded, light-switchable Phy-PIF interaction module which, because it has a properly titrated tight but reversible interaction, has the potential to be applied to control any live cell process that is dependent on a recruitment event. Unlike classical uncaging techniques, photoreversibility allows our system to defeat diffusive spreading by using patterned light. Furthermore, the direct relationship between the recruited fluorescent fraction and signalling activity also enables measurable 'dosage' of signalling flux for quantitative perturbations. We show here that the system works robustly in mammalian cells with external PCB, extending previous demonstrations in yeast<sup>10</sup> and its natural domain in plants, indicating that it is compatible with most eukaryotic cells. For genetically

'extrusion' of lamellipodia in live NIH3T3 cells (epifluorescence imaging, EPI) was demonstrated by globally irradiating the whole sample with an infrared (750 nm) light source while focusing a red (650 nm) laser on to a small portion of the cell as in Fig. 2a and slowly extending this red-targeted region from the cell body. Superimposed outlines of the cell show directed extension 30 μm along the line of light movement (Supplementary Movie 7). **d**, Cdc42-GTP binding domain (WASP-GBD) linked to mCherry was used to measure the 'response function' of intersectin-DH-PH recruitment over several iterations in time and in space at equilibrium (Supplementary Movie 11). Scale bars in **c** and **d**, 20 μm.

manipulable cells, it is, in principle, simple to include genes for enzymes that will generate PCB from haem or biliverdin<sup>26</sup>.

The high spatial and temporal resolution of light control allows this module to function as a novel analytical tool, in which highly complex spatial or temporal patterns can be used to drive a process. We have also demonstrated here how this module can be used as a high-resolution control module to sculpt cell shape in an unprecedented manner. Because of the generic nature of this interaction module, it is likely that it can be used to control an extremely broad range of cell biological processes without the need for laborious case-by-case protein engineering.

## METHODS SUMMARY

**Phycocyanobilin (PCB) purification.** PCB was extracted by methanolysis at 70 °C from protein precipitates of *Spirulina* cell lysate (Seltzer Chemical) that were pre-washed to remove other tetrapyrroles species. Free PCB was handled under a green safelight ( $\lambda_{\max}$  of 550 nm).

**Light control experiments.** NIH3T3 cells transiently transfected with the phytochrome and PIF constructs were pre-incubated in the dark with 5 μM PCB for 30 min and then washed before experiments. Non-coherent control-light frequencies were obtained by filtering white-light sources with 650-nm and 750-nm 20-nm band-pass filters (Edmund Optics) or a near-infrared RG9 glass filter (Newport). For morphology experiments, cells were serum-depleted (1% Bovine Calf Serum) for at least 12 h before imaging.

Received 8 July; accepted 24 August 2009.

Published online 13 September 2009.

1. Szobota, S. *et al.* Remote control of neuronal activity with a light-gated glutamate receptor. *Neuron* 54, 535–545 (2007).

2. Boyden, E. S., Zhang, F., Bamberg, E., Nagel, G. & Deisseroth, K. Millisecond-timescale, genetically targeted optical control of neural activity. *Nature Neurosci.* **8**, 1263–1268 (2005).
3. Han, X. & Boyden, E. S. Multiple-color optical activation, silencing, and desynchronization of neural activity, with single-spike temporal resolution. *PLoS One* **2**, e299 (2007).
4. Mettetal, J. T., Muzzey, D., Gómez-Urbe, C. & van Oudenaarden, A. The frequency dependence of osmo-adaptation in *Saccharomyces cerevisiae*. *Science* **319**, 482–484 (2008).
5. Bennett, M. R. *et al.* Metabolic gene regulation in a dynamically changing environment. *Nature* **454**, 1119–1122 (2008).
6. Ghosh, M. *et al.* Cofilin promotes actin polymerization and defines the direction of cell motility. *Science* **304**, 743–746 (2004).
7. Gorostiza, P. & Isacoff, E. Y. Optical switches for remote and noninvasive control of cell signaling. *Science* **322**, 395–399 (2008).
8. Levskaya, A. *et al.* Synthetic biology: engineering *Escherichia coli* to see light. *Nature* **438**, 441–442 (2005).
9. Lee, J. *et al.* Surface sites for engineering allosteric control in proteins. *Science* **322**, 438–442 (2008).
10. Shimizu-Sato, S., Huq, E., Tepperman, J. M. & Quail, P. H. A light-switchable gene promoter system. *Nature Biotechnol.* **20**, 1041–1044 (2002).
11. Quail, P. H. Phytochrome photosensory signalling networks. *Nature Rev. Mol. Cell Biol.* **3**, 85–93 (2002).
12. Ni, M., Tepperman, J. M. & Quail, P. H. Binding of phytochrome B to its nuclear signalling partner PIF3 is reversibly induced by light. *Nature* **400**, 781–784 (1999).
13. Khanna, R. *et al.* A novel molecular recognition motif necessary for targeting photoactivated phytochrome signaling to specific basic helix-loop-helix transcription factors. *Plant Cell* **16**, 3033–3044 (2004).
14. Tyszkiewicz, A. B. & Muir, T. W. Activation of protein splicing with light in yeast. *Nature Methods* **5**, 303–305 (2008).
15. Leung, D. W., Otomo, C., Chory, J. & Rosen, M. K. Genetically encoded photoswitching of actin assembly through the Cdc42-WASP-Arp2/3 complex pathway. *Proc. Natl Acad. Sci. USA* **105**, 12797–12802 (2008).
16. Su, Y. & Lagarias, J. C. Light-independent phytochrome signaling mediated by dominant GAF domain tyrosine mutants of *Arabidopsis* phytochromes in transgenic plants. *Plant Cell* **19**, 2124–2139 (2007).
17. Heo, W. D. *et al.* PI(3,4,5)P<sub>3</sub> and PI(4,5)P<sub>2</sub> lipids target proteins with polybasic clusters to the plasma membrane. *Science* **314**, 1458–1461 (2006).
18. Al-Sady, B., Ni, W., Kircher, S., Schäfer, E. & Quail, P. H. Photoactivated phytochrome induces rapid PIF3 phosphorylation prior to proteasome-mediated degradation. *Mol. Cell* **23**, 439–446 (2006).
19. Genoud, T. *et al.* FHY1 mediates nuclear import of the light-activated phytochrome A photoreceptor. *PLoS Genet.* **4**, e1000143 (2008).
20. Chen, M., Tao, Y., Lim, J., Shaw, A. & Chory, J. Regulation of phytochrome B nuclear localization through light-dependent unmasking of nuclear-localization signals. *Curr. Biol.* **15**, 637–642 (2005).
21. Inoue, T., Heo, W. D., Grimley, J. S., Wandless, T. J. & Meyer, T. An inducible translocation strategy to rapidly activate and inhibit small GTPase signaling pathways. *Nature Methods* **2**, 415–418 (2005).
22. Wang, S. *et al.* All optical interface for parallel, remote, and spatiotemporal control of neuronal activity. *Nano Lett.* **7**, 3859–3863 (2007).
23. Castellano, F. *et al.* Inducible recruitment of Cdc42 or WASP to a cell-surface receptor triggers actin polymerization and filopodium formation. *Curr. Biol.* **9**, 351–361 (1999).
24. Suh, B., Inoue, T., Meyer, T. & Hille, B. Rapid chemically induced changes of PtdIns(4,5)P<sub>2</sub> gate KCNQ ion channels. *Science* **314**, 1454–1457 (2006).
25. Inoue, T. & Meyer, T. Synthetic activation of endogenous PI3K and Rac identifies an AND-gate switch for cell polarization and migration. *PLoS One* **3**, e3068 (2008).
26. Gambetta, G. A. & Lagarias, J. C. Genetic engineering of phytochrome biosynthesis in bacteria. *Proc. Natl Acad. Sci. USA* **98**, 10566–10571 (2001).

**Supplementary Information** is linked to the online version of the paper at [www.nature.com/nature](http://www.nature.com/nature).

**Acknowledgements** We thank B. El-Sady, J. Tepperman, K. Thorn, G. Kapp and members of the Voigt, Weiner and Lim laboratories for assistance and discussion. We thank Molecular Devices and Photonics Instruments for the loan and customization of a Mosaic spatial light modulator. Data for this study were acquired at the Nikon Imaging Center at UCSF. This work was supported by a NSFGR fellowship (A.L.); NIH R01 GM084040 and Searles Scholar Award.(O.D.W.); Packard Fellowship, the Howard Hughes Medical Institute, and NIH grants GM55040, GM62583 and EY016546 (NIH Roadmap Nanomedicine Development Centers) (W.A.L.); Pew Fellowship, the Office of Naval Research, Packard Fellowship, NIH EY016546, NIH AI067699, NSF BES-0547637, UC-Discovery and the SynBERC NSF ERC (C.A.V.).

**Author Contributions** Concept was conceived by A.L., W.A.L. and C.A.V.; experiments were executed by A.L.; spatiotemporal microscopy methods were developed by A.L. and O.D.W.; all authors were involved in interpretation of results and preparation of the manuscript.

**Author Information** Plasmids will be available from Addgene (<http://www.addgene.org>). Reprints and permissions information is available at [www.nature.com/reprints](http://www.nature.com/reprints). Correspondence and requests for materials should be addressed to W.A.L. ([lim@cmp.ucsf.edu](mailto:lim@cmp.ucsf.edu)).